Cone-Beam Image Reconstruction
by Moving Frames

Xiaochun Yang[1] and Berthold K.P. Horn[2]

[1] Biovisum, Inc., Boston MA 02116, USA
`xiaochun@biovisum.com`
[2] MIT EECS and CSAIL, Cambridge MA 02139, USA
`bkph@csail.mit.edu`

Abstract. In this paper, we present a new algorithmic paradigm for cone-beam image reconstruction. The new class of algorithms, referred to as cone-beam reconstruction by moving frames, enables numerical implementation of exact cone-beam inversion using its intrinsic geometry. In particular, our algorithm allows a 3-D discrete approach to the differentiation-backprojection operator on the curved manifolds appearing in all analytical cone-beam inverse formulations. The enabling technique, called the method of moving frames, has been popular in the computer vision community for many years [3]. Although cone-beam image reconstruction has come from a different origin and has been until now developed along very different lines from computer vision algorithms, we can find analogies in their line-and-plane geometry. We demonstrate how the moving frame technique can be made into a ubiquitous and powerful computational tool for designing and implementing more robust and more accurate cone-beam reconstruction algorithms.

1 Introduction

As innovations in X-ray detector technology made it to the front lines of computerized tomography (CT) in the late 1980s, the idea of 3-D cone-beam CT triggered the dramatic onset of a new revolution in volumetric imaging. Facilitated by the slip-ring technology and detector advances, the cone-beam system is able to use multi-row area detectors rather than detectors aligned on a single linear array in the older, slice-at-a-time 2-D machines, significantly increasing the information throughput and leading to faster, more nearly isotropic data collection. As a result, the cone-beam CT has a great potential to dramatically improve the speed and accuracy of CT imaging while lowering the hazardous radiation exposure. Accurate imaging ensures better diagnosis; high throughput leads to more efficient use of CT machines and hence lowers scan costs. As the CT industry works towards achieving its next milestone, cone-beam CT is now at the center of attention and the subject of intensive study.

A typical cone-beam imaging system generates a set of cone-beam projections from a radiation source to an area detector. Each cone-beam projection image provides the integral of the object density, denoted by f, along the straight lines

from the source to points on the detector surface. As the source-detector pair rotates and translates around the object, a collection of line integrals with the source point moving along a curve are obtained. The curve followed by the source relative to the scanned object is called the source orbit or the scan path. The task of cone-beam reconstruction is to invert the line integrals obtained from a series cone-beam projections and recover the density distribution f.

Approaches to cone-beam reconstruction can be categorized as either approximate or exact. Approximate reconstruction methods, such as Feldkamp's algorithm [4], are usually extensions of 2-D fan-beam or parallel-beam reconstruction methods. They are simpler to implement, but have serious limitation in reconstruction accuracy. Exact reconstruction methods are instead based on exact cone-beam inversion formula. Before 1991, three inversion formulae had been derived by Tuy [15], Smith [14] and Grangeat [5]. For a decade, engineers and researchers worked to reduce the above mathematical formulism into practical implementation but encountered many difficulties. The most complex and expensive computational step, the differentiation-backprojection operation, acts on curved surface in a fashion that was not completely understood.

In 2001, cone-beam inversion formulae derived by Katsevich [9] and Yang [16] considerably simplified cone-beam reconstruction. Katsevich gave the first helical cone-beam inversion formula as an iterated 2-D integral which suggests the minimum use of data. With this formulation, however, some integral parameter has implicit dependency on the scanning geometry and a set of nonlinear equations need to be solved. Yang instead reformulated the 3-D Radon inverse for general trajectories. The result is a reduction of the 3-D backprojection into a series of 2-D backprojections – it is the first explicit cone-beam inverse. More recently, Katsevich extended his original formulation to general trajectories [10].

Underlying Katsevich and Yang's cone-beam inverse reconstructions are two intrinsic vector spaces: one is the projective space of lines or planes passing through a point, called a fiber; the other is the fiber bundle constituting all the fibers emitting from a 3-D curve. These vector spaces are curved, differentiable manifolds. Inverse reconstruction integrates and differentiates functions defined on said vector spaces. Currently, there is no general theory for numerical calculus on curved manifold. In this paper, we explore the mechanism for integration and differentiation on the manifolds of lines and planes described above and provide a new computational framework for cone-beam image reconstruction.

The remainder of this paper is organized as follows. Section 2 studies the topological structure and varied coordinate representations of the vector spaces arising in cone-beam image reconstruction. Section 3 presents a novel reconstruction algorithm using the method of moving frames. In particular, implementation of the exterior derivative in Katsevich and Yang's formulae is discussed in detail.

2   Integral Geometry in Cone-Beam CT

There are three distinguished spaces when we process cone-beam image data. First is the object space in which the 3-D density function f is to be evaluated. The object space is an Euclidean space, denoted by $\mathbf{E}^3$.

Next is the source orbit, assumed to be a smooth and differentiable 3-D curve, is a 1-D manifold, denoted by $\mathbf{C}^1$. Assume that the source orbit is parameterized in the Euclidean coordinate by $\boldsymbol{\Phi}(\lambda) = (\phi_1(\lambda), \phi_2(\lambda), \phi_3(\lambda))$ with $\lambda \in \Lambda$. Given λ, one can determine not only the position of the source in the Euclidean space $\mathbf{E}^3$, but also the local properties, such as the tangent and curvature, of the manifold $\mathbf{C}^1$ at $\boldsymbol{\Phi}(\lambda)$. In this sense, λ also acts as a local coordinate of the source orbit when viewed on the 1-parameter manifold $\mathbf{C}^1$.

A third space is the space constituting all the projective lines emitting from a 3-D curve, denoted by $\mathbf{T} := \sum_{\lambda \in \Lambda} \mathbf{P}_\lambda^2$ where $\mathbf{P}_\lambda^2$ stands for the 2-D projective line-space projected from a single source point $\boldsymbol{\Phi}(\lambda)$. According to the line-and-plane duality in 2-D projective space [12], the projective space of lines, $\mathbf{P}_\lambda^2$, is interchangeable with the projective space of planes with the same projection center. Denote the projective space of planes with center at $\boldsymbol{\Phi}(\lambda)$ by $\widehat{\mathbf{P}}_\lambda^2$. Denote the total space of projective planes intersecting $\mathbf{C}^1$ by $\widehat{\mathbf{T}} := \sum_{\lambda \in \Lambda} \widehat{\mathbf{P}}_\lambda^2$.

Note that $\mathbf{E}^3$, $\mathbf{C}^1$, $\mathbf{P}_\lambda^2$ and $\widehat{\mathbf{P}}_\lambda^2$ are all embedded in the Euclidean 3-space. Points in these spaces and their geometric relationship can be described in the language of coordinates.

2.1   Euclidean Moving Frames

The object space $\mathbf{E}^3$ can be represented in the Cartesian coordinate with an origin denoted by O. This coordinate system will be referred to as the global Euclidean frame – it is fixed with respect to the object.

As the radiation source moves around the object, the orientation of the detector surface changes accordingly. In practice, the detector surface may be curved. For convenience of exposition, we replace the detector array with an image plane that closely approximates the detector surface. A coordinate transformation is needed to map every point on the real detector surface onto the image plane.

Moving Frames and Local Coordinates. Assume that the source-to-detector distance is fixed. Also assume that the two perpendicular axes on the image plane evolve smoothly during the source-detector motion. A local Euclidean coordinate can be conveniently set up for each projection with the origin at the source point, two axes aligned with the axes of the image plane, and the third axis aligned with the perpendicular line from the source to the image plane. Let O_I be the intersecting point where the perpendicular line from the source to the image plane meets the image plane.

Denote by $\big\{ \boldsymbol{\Phi}(\lambda) : \boldsymbol{u}(\lambda), \boldsymbol{v}(\lambda), \boldsymbol{w}(\lambda) \big\}$ ($\lambda \in \Lambda$) the series of local Euclidean frames attached to the source orbit where λ is considered as an index and $\boldsymbol{u}(\lambda)$,

$v(\lambda)$, $w(\lambda)$ are the three orthonormal basis vectors expressed in the global Euclidean coordinate. As λ ranges in Λ, the smooth evolution of u and v ensures the smooth evolution of w, since w can be computed from $u \times v$.

The sequence of orthonormal local coordinates described above are called the Euclidean moving frames. Construction of the moving frame bases generates a set of 3-by-3 orthonormal matrices, *i.e.,* $\mathbf{R}(\lambda) = \big(u(\lambda), v(\lambda), w(\lambda)\big)$ $(\lambda \in \Lambda)$, which are associated with a set of consecutive rotations. Given a point $x \in \mathbf{E}^3$, assume x' is the corresponding local coordinate in the Euclidean frame indexed by λ. The coordinate transform from x' to x and its inverse are given by

$$x = \mathbf{R}(\lambda)x' + \mathbf{\Phi}(\lambda), \tag{1}$$

$$x' = \mathbf{R}(\lambda)^{-1}\big(x - \mathbf{\Phi}(\lambda)\big). \tag{2}$$

It is clear that every point in the object space has simultaneously a global Euclidean coordinate as well as a series of local Euclidean coordinates.

Construction of Moving Frames. Construction of the moving frames is fairly general, flexible and can be applied to a wide selections of source orbits and detector orientations. However, in practice, detector orientations are constrained in the sense that its movement needs to be synchronized with the source and the synchronized motion is under the control of rigid translation and rotation.

To produce a smooth evolution of the moving frame bases as the source-detector moves around the object, we can make use of the source orbit equation and express the local Euclidean bases in terms of the vector components of $\mathbf{\Phi}(\lambda)$. For example, if the rotational axis of the source orbit is fixed, as in traditional CT where source and detector are mounted on a cylindrical gantry that rotates around a fixed axis, we can align one of the basis vectors, say v, to the rotational axis (shown as the vertical axis in Fig. 1) and let the other two axes synchronize with the rotation of the source when viewed from a plane perpendicular to the rotational axis. This yields the following orthonormal basis:

$$\begin{cases} u(\lambda) = \dfrac{1}{\sqrt{\phi_1^2(\lambda) + \phi_2^2(\lambda)}}\Big(-\phi_2(\lambda), \phi_1(\lambda), 0\Big) \\ v(\lambda) = \Big(0,\ 0,\ 1\Big) \\ w(\lambda) = \dfrac{1}{\sqrt{\phi_1^2(\lambda) + \phi_2^2(\lambda)}}\Big(\phi_1(\lambda), \phi_2(\lambda), 0\Big) \end{cases}. \tag{3}$$

Alternatively, if spherical symmetry characterizes the scanning geometry, such as in C-arm CT where the radiation source is confined on a spherical surface, then one of the moving frame basis vectors, say w, can be aligned with the position vector, $\mathbf{\Phi}(\lambda)$, and the other two axes are made dependent on both the position vector and the local tangent of the source orbit (see Fig. 2), *i.e.,*

$$\begin{cases} w(\lambda) = \dfrac{\mathbf{\Phi}(\lambda)}{|\mathbf{\Phi}(\lambda)|} \\ v(\lambda) = \dfrac{w \times \mathbf{\Phi}'(\lambda)}{|w \times \mathbf{\Phi}'(\lambda)|} \\ u(\lambda) = v \times w \end{cases}. \tag{4}$$
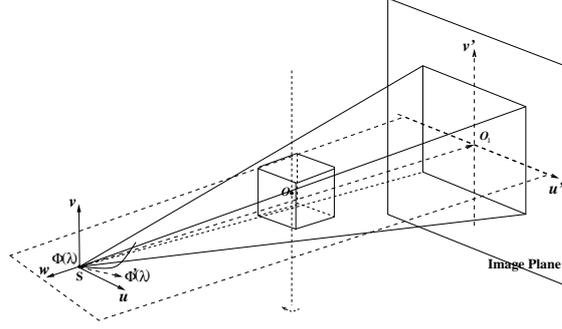
Fig. 1. *Moving frame (a).*
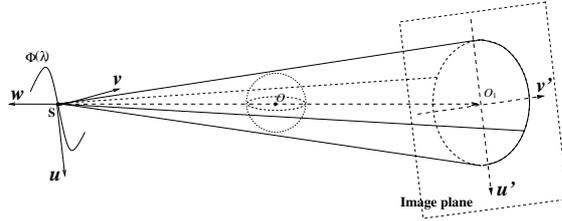
Fig. 2. *Moving frame (b).*

In both cases, cone-beam system design includes an alignment step to align the axes of the image plane with the designated axes.

Coordinate of Lines and Planes. In a local projection frame, we consider only the lines and planes passing through the source point $\mathbf{\Phi}(\lambda)$ and the support of f. In the case of lines, the global Euclidean coordinates of the intersecting points between the lines and the image plane can be obtained from their local Euclidean coordinates via Eqn. (1). Consequently, the directions of the lines, denoted by $\boldsymbol{\alpha} \in \mathbf{S}^2$, can also be expressed in the global Euclidean coordinates. We refer to $(\lambda, \boldsymbol{\alpha})$ as the projective coordinate of lines emitting from $\mathbf{\Phi}(\lambda)$.

In the case of the planes, we note that a plane can be identified by two distinctive lines on that plane. Assume P_1 and P_2 are two points on the intersecting line between a given plane and the image plane. The projective coordinates of two lines connecting the source to P_1 and P_2 can be calculated as previously described. Denote the projective coordinates of the said lines by $(\lambda, \boldsymbol{\alpha}_1)$ and $(\lambda, \boldsymbol{\alpha}_2)$ respectively. The unit normal of the given plane, denoted by $\boldsymbol{\beta}$, is perpendicular to both $\boldsymbol{\alpha}_1$ and $\boldsymbol{\alpha}_2$. Therefore, $\boldsymbol{\beta} = \boldsymbol{\alpha}_1 \times \boldsymbol{\alpha}_2 / |\boldsymbol{\alpha}_1 \times \boldsymbol{\alpha}_2|$. The radial distance of the plane, denoted by l, can be evaluated as $l = \mathbf{\Phi}(\lambda) \cdot \boldsymbol{\beta}$. The coordinate $(l, \boldsymbol{\beta})$ determines the position of a plane seen in the global Euclidean coordinate.

2.2   Integral Transforms on Projective Spaces

Each cone-beam projection consists of rays emitting from a source point. The pencil of rays forms a 2-D projective space. Two integral transforms can be defined on the projective 2-space of lines and its dual, namely the projective 2-space of planes, respectively. Inverting integral transforms on various geometric spaces is the main subject of study in integral geometry.

Divergent Ray Transform. For a fixed source position, say $\boldsymbol{\Phi}(\lambda)$, cone-beam projection maps points in $\mathbf{E}^3$ onto $\mathbf{P}_\lambda^2$ with the equivalence relation:

$$\boldsymbol{\Phi}(\lambda) + \boldsymbol{\alpha} \sim \boldsymbol{\Phi}(\lambda) + r\boldsymbol{\alpha} \quad \text{for } \boldsymbol{\alpha} \in \mathbf{S}^2, \ r \in \mathbb{R} \text{ and } r \neq 0. \tag{5}$$

The pair $(\lambda, \boldsymbol{\alpha})$ identifies a line in the Euclidean 3-space.

   Assume that the density function f has a finite support, $\Omega \in \mathbb{R}^3$, and the source orbit $\boldsymbol{\Phi}(\lambda)$ is outside the convex hull of Ω. The *divergent ray transform* of f is by definition the integrals of f along the half-lines starting at $\boldsymbol{\Phi}(\lambda)$ which is a measurement available from the cone-beam image:

$$Df(\lambda, r\boldsymbol{\alpha}) := \int_0^{+\infty} f(\boldsymbol{\Phi}(\lambda) + t\boldsymbol{\alpha}) \, dt, \quad \boldsymbol{\alpha} \in \mathbf{S}^2, \ r \in \mathbb{R}. \tag{6}$$

Cone-beam reconstruction is to recover f from Df.

Radon Transform. In the 2-D projective space of lines, every two distinctive lines determine a unique plane; every two distinctive planes determine a unique line. Thus, lines and planes are *dual* in the 2-D projective space. This duality relation is important in that it makes the integral transform along the lines interchangeable with some integral transform over the planes.

   We can write a plane in $\mathbb{R}^3$ as

$$\boldsymbol{L}_{l,\boldsymbol{\beta}} := \Big\{ \boldsymbol{x} \in \mathbb{R}^3 \mid \boldsymbol{x} \cdot \boldsymbol{\beta} = l, \ l \geq 0, \ \boldsymbol{\beta} \in \mathbf{S}^2 \Big\}, \tag{7}$$

where $\boldsymbol{\beta}$ is the unit normal of the plane and l is the perpendicular distance of the plane from the origin. The space of all the planes in $\mathbb{R}^3$ is called the Radon space. Radon space is a projective 3-space, denoted by $\mathbf{P}^3$.

   The *Radon transform* of f is defined as the set of integrals of f over all the planes in $\mathbb{R}^3$ which can be expressed as a function of two parameters (l and $\boldsymbol{\beta}$):

$$Rf(l, \boldsymbol{\beta}) := \int_{\boldsymbol{x} \in \{ \boldsymbol{x} \mid \boldsymbol{x} \cdot \boldsymbol{\beta} = l \}} f(\boldsymbol{x}) \, d\boldsymbol{x}. \tag{8}$$

If Rf is known on all the planes passing by the support of f, then f can be reconstructed from the 3-D Radon inverse [6,13]:

$$f(\boldsymbol{x}) = -\frac{1}{8\pi^2} \int_{\mathbf{S}^2} \frac{\partial^2 Rf(l, \boldsymbol{\beta})}{\partial l^2} \bigg|_{l=\boldsymbol{x} \cdot \boldsymbol{\beta}} d\boldsymbol{\beta}. \tag{9}$$

However, in cone-beam projection, only the divergent ray transform is available, not the Radon transform. In order to use Eqn. (9) to recover the function value at point $\boldsymbol{x}$, the second-order radial derivative of the Radon transform needs to be obtained on all or almost all planes through $\boldsymbol{x}$. Grangeat's Fundamental Relation [5] provides an important link from the divergent ray transform to the Radon transform. According to the Fundamental Relation, the first-order radial derivative of the Radon transform on a plane can be calculated from the weighted integral of the divergent ray transform along projective lines on the given plane as well as its adjacent planes within the same projection. The second radial derivative of the Radon transform can then be evaluated by differentiating the first radial derivative of the Radon transform over parallel planes.

Cone-beam inversion formulae earlier derived by Tuy [15] and Smith [14] have also been linked to Eqn. (9) [2,16]. It turns out that exact cone-beam reconstruction based on Eqn. (9) requires source orbit to meet the data sufficiency condition, *i.e.*, all or almost all planes passing by the support of f intersect with the source orbit [5,14,15,16].

Transform Spaces $\mathbf{T}$ and $\widehat{\mathbf{T}}$ as Fiber Bundles. From each point lying on the source orbit grows a 2-D projective space of lines, $\mathbf{P}_\lambda^2$, as well as a 2-D projective space of planes, $\widehat{\mathbf{P}}_\lambda^2$. The transform spaces $\mathbf{T}$ and $\widehat{\mathbf{T}}$ are unions of all $\mathbf{P}_\lambda^2$ and all $\widehat{\mathbf{P}}_\lambda^2$ projected from the source orbit respectively. The geometric structure of $\mathbf{T}$ and $\widehat{\mathbf{T}}$ is called a *fiber bundle* in differential geometry [11]. The source curve $\mathbf{C}^1$ is called the base space and $\mathbf{P}_\lambda^2$ or $\widehat{\mathbf{P}}_\lambda^2$ are the fibers. Points in $\mathbf{T}$ and $\widehat{\mathbf{T}}$ correspond to lines and planes when viewed in the Euclidean space.

Recall from our earlier discussion, lines and planes emitting from $\boldsymbol{\Phi}(\lambda)$ ($\lambda \in \Lambda$) can be identified by the direction of the lines, $\boldsymbol{\alpha} \in \mathbf{S}^2$, and the normal direction of the planes, $\boldsymbol{\beta} \in \mathbf{S}^2$, respectively. Assume $\left(\mathbf{S}^2; \ \alpha^i\right)$ is a basis for the fiber of lines, and $\left(\mathbf{S}^2; \ \beta^i\right)$ is a basis for the fiber of planes. Then, the Cartesian product of the bases from the base space and the fiber space, namely $\left(\Lambda; \ \lambda\right) \times \left(\mathbf{S}^2; \ \alpha^i\right)$ and $\left(\Lambda; \ \lambda\right) \times \left(\mathbf{S}^2; \ \beta^i\right)$, are local bases for $\mathbf{T}$ and $\widehat{\mathbf{T}}$.

Fiber bundle captures the underlying cone-beam scanning geometry concisely and precisely. Moreover, if the source orbit satisfies the data sufficiency condition, then $\widehat{\mathbf{T}} = \sum_{\lambda \in \Lambda} \widehat{\mathbf{P}}_\lambda^2$ is a covering space of the Radon space, $\mathbf{P}^3$ (reduced to contain only the planes intersecting the support of f). The *inclusion map* from each fiber $\widehat{\mathbf{P}}_\lambda^2$ to $\mathbf{P}^3$ is given by $\Pi_\lambda : \boldsymbol{\beta} \longrightarrow \left(l, \boldsymbol{\beta}\right)$ with $l = \boldsymbol{\Phi}(\lambda) \cdot \boldsymbol{\beta}$. Note that the same map transforms the local coordinate in $\widehat{\mathbf{T}}$ to the global coordinate in $\mathbf{P}^3$. However, the above mapping is not bijective, because some planes in the Radon space are repeated multiple times in $\widehat{\mathbf{T}}$. Denote by $M(\lambda, \boldsymbol{\beta})$ the number of times that the 2-D plane $\boldsymbol{L}_{\boldsymbol{\Phi}(\lambda) \cdot \boldsymbol{\beta}, \boldsymbol{\beta}}$ intersects with the source orbit. Then the same function $M(\lambda, \boldsymbol{\beta})$ depicts the number of times that the plane $\boldsymbol{L}_{\boldsymbol{\Phi}(\lambda) \cdot \boldsymbol{\beta}, \boldsymbol{\beta}}$ is repeated in $\widehat{\mathbf{T}}$. This $M(\lambda, \boldsymbol{\beta})$ is called the *redundancy function*.

Differential Structure and Connection. Both the base space and the fiber space are differentiable manifolds. Therefore, the fiber bundles $\mathbf{T}$ and $\widehat{\mathbf{T}}$ are differentiable. The coordinate from the base space, λ, serves as a *connection* in the fiber bundles in the following sense: as λ smoothly varying in a neighborhood, the disjoint fibers get connected and the result is a smooth manifold. For fixed $\boldsymbol{\alpha} \in \mathbf{S}^2$ and $\boldsymbol{\beta} \in \mathbf{S}^2$, displacement in λ indicates parallel translation of a line (with direction $\boldsymbol{\alpha}$) or a plane (with normal direction $\boldsymbol{\beta}$).

In $\widehat{\mathbf{T}}$, the first local coordinate λ relates to the first global coordinate l by the differentiable map $l = \boldsymbol{\Phi}(\lambda) \cdot \boldsymbol{\beta}$. Hence, $\partial/\partial l = (1/\boldsymbol{\Phi}'(\lambda) \cdot \boldsymbol{\beta})\partial/\partial\lambda$. We can visualize the differentiation process over parallel planes by taking an infinitesimal step along the tangent direction of the source orbit – almost always we can find a plane parallel to the one we start from, except if the initial plane contains the tangent line. We call these exceptional planes the *defects* in the structure of the fiber bundle $\widehat{\mathbf{T}}$. Although differentiation over parallel planes breaks at the defective planes in $\widehat{\mathbf{T}}$, it can still be carried out in the Radon space, $\mathbf{P}^3$, with respect to the radial distance l. In the Radon space, the global coordinate l is a more stable benchmark for parallelism in planes than the local coordinate λ.

3   Exact Cone-Beam Reconstruction

Early algorithm development for exact cone-beam reconstructions is heavily based on inversion formulae derived by Tuy [15], Smith [14] and Grangeat [5]. Although varying in computational cost and stability, they share an important structural similarity in that they all inherited the differentiation-backprojection operator from the 3-D Radon inverse. They differ in the underlying intermediate functions linking the divergent ray transform to the Radon transform [2,16].

For nearly ten years, exact and efficient implementation of the three inversion formulae has encountered difficulties. This is mainly because the 3-D differentiation-backprojection operation has implicit dependency on the scanning parameter, λ, and discretization can not be easily introduced.

3.1   Inversion Formulae by Yang and Katsevich

Motivated by the similarity displayed in Tuy, Smith and Grangeat's inverse formulations, Yang investigated the topological structure of the Radon space, which is the transform space, and discovered two prevailing geometric constraints underlying cone-beam reconstruction [16]:

- First, within each cone-beam projection, all the planes passing through a particular projection line have normals perpendicular to that line; therefore, backprojection orientation is confined to a unit circle. The reduction of backprojection from 3-space to 2-space simplifies the reconstruction.
- Second, as the source moves along the orbit, backprojection orientation on the unit circle undergoes a rigid rotation. As long as the source orbit satisfies the data sufficiency condition, one can decompose 3-D backprojection into a series of 2-D backprojections in accordance with the scanning geometry.

This leads to the following decomposed 3-D Radon inverse:

$$f(\boldsymbol{x}) = -\frac{1}{8\pi^2} \int_\Lambda \left\{ \int_{\boldsymbol{\beta} \in \left\{ \boldsymbol{x} - \boldsymbol{\Phi}(\lambda) \right\}^\perp, \ \boldsymbol{\beta} \in \mathbf{S}^2} R'' f(\boldsymbol{\Phi}(\lambda) \cdot \boldsymbol{\beta}, \boldsymbol{\beta}) \frac{|\boldsymbol{\Phi}'(\lambda) \cdot \boldsymbol{\beta}|}{M(\lambda, \boldsymbol{\beta})} \, d\boldsymbol{\beta} \right\} \, d\lambda, \quad (10)$$

in which, $\left\{ \boldsymbol{x} - \boldsymbol{\Phi}(\lambda) \right\}^\perp$ denotes the plane perpendicular to the projection ray $\boldsymbol{x} - \boldsymbol{\Phi}(\lambda)$ and through the origin. The outer integral integrates over the source orbit; the inner integral is a 2-D backprojection – with each cone-beam projection, there is only one 2-D backprojection that needs to be performed along each projection ray and the resulting value is assigned to all the points lying on that ray with the same weight. Coupled with Grangeat's Fundamental Relation, Eqn. (10) provides an explicit solution for cone-beam reconstruction.

More recently, Katsevich derived a new general cone-beam inversion formula which is extended from his inverse formulation for truncated helical cone-beam problem [9]. The new inverse is an iterated double integral [10]:

$$f(\boldsymbol{x}) = -\frac{1}{8\pi^2} \int_\Lambda \left\{ \frac{\sum c_m(\lambda, \boldsymbol{x})}{|\boldsymbol{x} - \boldsymbol{\Phi}(\lambda)|} \int_0^{2\pi} \frac{\partial}{\partial \lambda'} Df(\boldsymbol{\Phi}(\lambda'), \cos\gamma \, \boldsymbol{\alpha}(\lambda, \boldsymbol{x}) + \right.$$
$$\left. \sin\gamma \, \boldsymbol{\alpha}^\perp(\lambda, \boldsymbol{x}, \theta_m)) \mid_{\lambda'=\lambda} \frac{d\gamma}{\sin\gamma} \right\} \, d\lambda. \quad (11)$$

Again, the outer integral integrates along the source orbit. The inner integral, however, is a 1-D integral that integrates over a plane determined by λ, $\boldsymbol{x}$, θ_m and the integral parameter γ denotes the polar angle on this plane. Furthermore, $\boldsymbol{\alpha}$ denotes the unit vector in the direction of the projection ray, $\boldsymbol{x} - \boldsymbol{\Phi}(\lambda)$, and $\boldsymbol{\alpha}^\perp$ is a unit vector perpendicular to $\boldsymbol{\alpha}$; the polar angle in the plane perpendicular to $\boldsymbol{\alpha}$ and through the origin is θ. At θ_m $(m = 1, 2, ...)$, $\boldsymbol{\alpha}$ and $\boldsymbol{\alpha}^\perp$ are both lying on the integration plane which is a critical plane in the sense that it produces a jump in $c(\lambda, \boldsymbol{x})$, a weight function related to the number of intersections of a plane passing through $\boldsymbol{x}$ and $\boldsymbol{\Phi}(\lambda)$ with the source orbit. Note, the jumps in $c(\lambda, \boldsymbol{x})$ occur only at finite number of θ_m's. To find these θ_m's and the corresponding critical planes, a set of nonlinear equations need to be solved. The critical plane contains either a tangent of $\boldsymbol{\Phi}(\lambda)$ or an end point of $\boldsymbol{\Phi}(\lambda)$. Interestingly, a large number of the integration planes thus selected correspond to the defective structure on the fiber bundle $\widehat{\mathbf{T}}$. This connection can be further addressed. See [10] for more detailed explanation of the inversion formula.

To carry out numerical implementation of Eqn. (10)-(11), it is important that the discretization step preserves the geometric relationship among the points, lines and planes hidden in the formulae. Fiber bundle geometry provides an ideal setting for such a discretization: discretizing the outer integral corresponds to discretizing the source orbit, the base space; discretizing the inner integral corresponds to discretizing the 2-D projective spaces of planes (Eqn. (10)) and lines (Eqn. (11)) which are the fibers. The second radial derivative in $R'' f$ (Eqn. (10)) and the derivative of Df with respect to λ (Eqn. (11)), on the other hand, are performed over parallel planes and lines across projections. It is clear that appropriate coordinates are needed in each space encountered in order to facilitate the discretization.

3.2   A Discrete Approach: Reconstruction by Moving Frames

Yang and Katsevich's formulae share a common three-step procedure which is carried out repeatedly for a sequence of cone-beam projections. The three steps are: integration on the fiber space – it corresponds to the inner integral; differentiation across neighboring projections, *i.e.*, over parallel planes (Eqn. (10)) or parallel lines (Eqn. (11)); backprojection assigning results from the first two steps to points along each projection ray – it is also performed in the fiber space. There are extra steps in each formula need to be performed, such as evaluation of $R'f$ from Df via Fundamental Relation (for Eqn. (10)), and finding the critical planes by solving a set of nonlinear equations (for Eqn. (11)), etc. To save space, however, we will focus our discussion on the three-step process.

Consider the orthonormal moving frames $\left\{ \mathbf{\Phi}(\lambda); \boldsymbol{u}(\lambda), \boldsymbol{v}(\lambda), \boldsymbol{w}(\lambda) \right\}$ ($\lambda \in \Lambda$) with the origin attached to the source orbit and the basis vectors determined by the local properties of $\mathbf{\Phi}(\lambda)$ (as discussed in Section 2.1). For some fixed λ, the local projective coordinates of lines and planes passing by $\mathbf{\Phi}(\lambda)$ can be obtained from the local Euclidean coordinates of points on the image plane. Thus, integration and differentiation on a fiber space present little challenge other than some irregularities in sampling. However, in order to perform differentiation over parallel lines or planes across projections, parallel lines or planes from neighboring projections need to be located. A coordinate that can flatly connect the set of parallel lines or planes, and can be transformed to and from the moving frame coordinates, is therefore needed. Such coordinate is identified in section 2.2 as the scan path parameter, λ, for lines and the radial distance, l, for planes. Displacement in λ or l indicates parallel translation if the direction of the line or the normal direction of the plane remains fixed. Consequently, differentiation can take place on the line bundle or the plane bundle which are curved manifolds.

Note that the pencil of lines and the pencil of planes growing out of a source point each forms a closed manifold. Each fiber space can be visualized by a unit sphere centered at the source position (see Fig. 3). A point on the sphere represents either a line or a plane passing through the source: the direction of the line or the normal of the plane coincides with the source-to-point line. In addition, for any two different source points, their corresponding fibers are disjoint. As λ smoothly varying along the source orbit, the disjoint fibers become connected to form a smooth and differentiable manifold. Now in the discrete approach, lines and planes from neighboring projections lie outside the closed fiber space of each other. Cross-projection differentiations is therefore an exterior differentiation. Differentiation inside the closed fiber space, for example, along the geodesics ζ and η (see Fig. 4), will *not* produce a *valid* exterior derivative.

To develop a discrete implementation of the exterior differentiation, parallel lines or planes from neighboring projections need to be aligned. This task is simpler in the case of lines, since two parallel lines have the same direction, *e.g.*, $\boldsymbol{\alpha}$, in the global Euclidean space, the rotating matrices representing the moving frames act on $\boldsymbol{\alpha}$ and generate orientations of the lines in the local frames. Thus, the intersections of the parallel lines with the corresponding image planes can be matched. To perform the geometric alignment for planes, we consider two
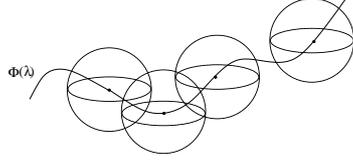
Fig. 3. *Fibers and connection.*
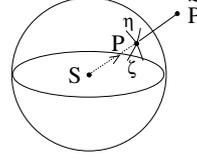
Fig. 4. *Exterior differentiation.*

consecutive projections and construct a set of planes in the second projection frame parallel to the set of planes in the first projection frame as follows.

Assume $(l_1, \boldsymbol{\beta})$ is the global coordinate of a plane from the first projection, with $l_1 = \boldsymbol{\Phi}(\lambda_1) \cdot \boldsymbol{\beta}$. In the second projection, the global coordinate of the plane passing through the source and parallel to $\boldsymbol{L}_{l_1, \boldsymbol{\beta}}$ is $(l_2, \boldsymbol{\beta})$ with $l_2 = \boldsymbol{\Phi}(\lambda_2) \cdot \boldsymbol{\beta}$. Denote by R the distance of the source from the rotational axis and D the distance of the source from the detector. Denote by (s, ϕ) the polar coordinate of the intersecting line between $\boldsymbol{L}_{l_2, \boldsymbol{\beta}}$ and the image plane (Fig.5). Let α be the angle between $\boldsymbol{L}_{l_2, \boldsymbol{\beta}}$ and the perpendicular from the source to the image plane. With the moving frames exemplified by Eqn. (4), the polar coordinate of the intersecting line between plane $\boldsymbol{L}_{l_2, \boldsymbol{\beta}}$ and the image plane can be expressed as

$$\begin{cases} s = D \dfrac{l_2}{\sqrt{R^2 - l_2^2}} \\ \phi = \arctan(\dfrac{\boldsymbol{\beta} \cdot \boldsymbol{v}}{\boldsymbol{\beta} \cdot \boldsymbol{u}}) \end{cases}, \tag{12}$$

in which s is obtained by eliminating α from $\sin \alpha = l_2/R$ and $\tan \alpha = s/D$.
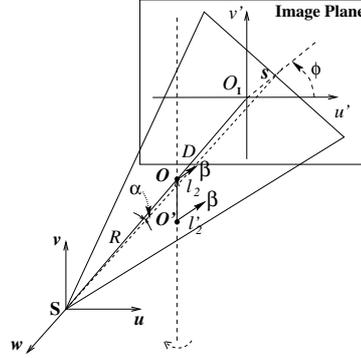
Fig. 5. *The second parallel plane intersecting the second image plane.*

With the moving frames exemplified by Eqn. (3), the perpendicular from the source to the image plane may not go through the origin. Instead, it meets the

rotational axis at O' (see Fig. 5). In this case, the radial distance of the plane, l_2, in Eqn. (12) shall be offset by $OO' \cdot \boldsymbol{\beta}$.

It is clear that the moving frames provide a perfect vehicle for accurate alignment of parallel lines and planes. As a result, robust evaluation of the exterior derivatives is made possible.

The method of moving frames is one giant pillar among several in Cartan's geometry [1] which holds a prominent position in modern differential geometry. The first known application of moving frame technique to computerized tomography appeared in [7,8] for 2-D fan-beam reconstruction. In the field of computer vision, the method of moving frames has been used to treat differential invariance of curves and other geometric invariance in a multi-view geometric setting similar to the one seen in cone-beam CT [3].

4   Conclusions

In this paper, the intrinsic geometry underlying analytical cone-beam inverse is revealed, as well as the associated coordinate systems and coordinate transforms. We have shown that the method of moving frames allows exact cone-beam inversion formula to be discretized on the intrinsic cone-beam geometry; thus, sampling and interpolation errors can be minimized. In addition, the moving frame technique makes reconstruction applicable to a wide selection of source orbits and detector orientations.

References

1. É. Cartan "La Méthode du Repère Mobile, la Théorie des Groupes Continus et les Espaces Généralisés." *Exposés de Géométrie No. 5*, Hermann, Paris, 1935
2. R. Clack and M. Defrise "Cone-beam Reconstruction by the use of Radon Transform Intermediate Functions. " *J. of Opt. Soc. Am. A.*, Vol. 11, No. 2, 1994, pp. 580–585
3. O. Faugeras "Cartan's Moving Frame Method and its Application to the Geometry and Evolution of Curves in the Euclidean, Affine and Projective Planes." *Applications of Invariance in Computer Vision, Second Joint European - US Workshop*, Ponta Delgada, Azores, Portugal, J. L. Mundy, A. Zisserman, D. A. Forsyth (Eds.), October 9–14, 1993, pp. 11–46,
4. L.A. Feldkamp, L.C. David and J.W. Kress "Practical Cone-beam Algorithm." *J. Opt. Soc. Am. A.*, Vol. 1, No. 6, 1984, pp. 612–619
5. P. Grangeat "Mathematical Framework of Cone Beam 3-D Reconstruction via the First Derivative of the Radon Transform." *Mathematical methods in tomography, Lecture notes in mathematics 1497*, 1991. pp. 66–97
6. S. Helgason *The Radon Transform*, 2nd Edition, Birkhäuser, 1999
7. B.K.P. Horn "Density Reconstruction using Arbitrary Ray Sampling Schemes." *Proceedings of the IEEE*, Vol. 66, No. 5, May 1978, pp. 551–562.
8. B.K.P. Horn "Fan-beam Reconstruction Methods." *Proceedings of the IEEE*, Vol. 67, No. 12, December 1979, pp. 1616–1623.
9. A. Katsevich "Theoretically exact FBP-type Inversion Algorithm for Spiral CT." *SIAM J. of App. Math.*, Vol. 62, 2002, pp. 2012–2026

10. A. Katsevich "A General Scheme for Constructing Inversion Algorithms for Cone Beam CT." *Int. J. of Math. and Math. Sci.*, 2003:21, pp. 1305–1321

11. S. Kobayashi and K. Nomizu *Foundations of Differential Geometry*, John Wiley & Sons Inc., 1963

12. *Geometric Invariance in Computer Vision*, MIT Press, J. L. Mundy and A. Zisserman (Eds.), 1992

13. F. Natterer *The Mathematics of Computerized Tomography*, John Wiley & Sons Ltd. and B. G. Teubner, Stuttgart, 1986

14. B.D. Smith "Image Reconstruction from Cone-beam Projections: Necessary and Sufficient Conditions and reconstruction methods." *IEEE Trans. Med. Imag.*, Vol. 4, 1985, pp. 14–25

15. H.K. Tuy "An Inversion Formula for Cone-beam Reconstruction." *SIAM J. Appl. Math*, Vol. 43, 1983, pp. 546–552

16. X. Yang "Geometry of Cone-beam Reconstruction." *Ph.D. Thesis*, Massachusetts Institute of Technology, Dept. of Mathematics, Cambridge, MA, September 2001